Volume 266, Issues 3–4 20 February 2008 ISSN 0012-821X

ELSEVIER

EARTH & PLANETARY SCIENCE LETTERS

Available online at www.sciencedirect.com
ScienceDirect
Earth and Planetary Science Letters 266 (2008) 332–344
EPSL
www.elsevier.com/locate/epsl

Seasonal variations of seismicity and geodetic strain in the Himalaya induced by surface hydrology

Pierre Bettinelli [a], Jean-Philippe Avouac [b,*], Mireille Flouzat [a], Laurent Bollinger [a], Guillaume Ramillien [c], Sudhir Rajaure [d], Som Sapkota [d]

[a] *Laboratoire de Détection et de Géophysique, CEA, BP12, Bruyères-le-Châtel, 91680, France*
[b] *California Institute of Technology, Tectonics Observatory, Geology and Planetary Sciences Division, MC 100-23, Pasadena, CA 91125, USA*
[c] *LEGOS, 31401 Toulouse, France*
[d] *National Seismological Centre, Department of Mines and Geology, Lainchaur, Kathmandu, Nepal*

Received 11 July 2007; received in revised form 9 November 2007; accepted 11 November 2007
Available online 22 November 2007
Editor: C.P. Jaupart

Abstract

One way to probe earthquake nucleation processes and the relation between stress buildup and seismicity is to analyze the sensitivity of seismicity to stress perturbations. Here, we report evidence for seasonal strain and stress (~2–4 kPa) variations in the Nepal Himalaya, induced by water storage variations which correlate with seasonal variations of seismicity. The seismicity rate is twice as high in the winter as in the summer, and correlates with stress rate variations. We infer ~10–20 kPa/yr interseismic stress buildup within the seismicity cluster along the high Himalaya front. Given that Earth tides exert little influence on Himalayan seismicity, the correlated seasonal variation of stress and seismicity indicates that the duration of earthquake nucleation in the Himalaya is of the order of days to month, placing constraints on faults friction laws. The unusual sensitivity of seismicity to small stress changes in the Himalaya might be due to high pore pressure at seismogenic depth.

Keywords: seismology; geodesy; tectonics; hydrology; Himalaya

1. Introduction

Background seismicity in the Himalaya is known to be driven by the slow, presumably steady-state, process of interseismic stress buildup in the period separating very large ($M>8$) earthquakes (Cattin and Avouac, 2000; Bollinger et al., 2004). However, strong seasonal fluctuations are observed, with winter seismicity twice as high as summer seismicity, on average (Bollinger et al., 2007). We analyze continuous geodetic data in order to investigate the cause of these variations, and derive implications for earthquake nucleation and fault rheology. Indeed, the earthquake nucleation process determines how seismicity responds to temporal or spatial variations in strain, whether these are related to coseismic deformation, postseismic relaxation, interseismic stress buildup, or periodic perturbations such as Earth tides (Dieterich et al., 2000; Dieterich, 1994, 1987; Lockner and Beeler,

* Corresponding author. Tel.: +626 395 4239; fax: +626 395 1740.
E-mail address: avouac@gps.caltech.edu (J.-P. Avouac).

0012-821X/$ - see front matter © 2007 Elsevier B.V. All rights reserved.
doi:10.1016/j.epsl.2007.11.021

1999; Beeler and Lockner, 2003; Stein, 1999; Toda et al., 2002; Perfettini and Avouac, 2004).

2. Background seismicity, secular strain and crustal structure

Local seismic monitoring in the Nepal Himalaya has revealed very intense background seismicity along the front of the high range (Pandey et al., 1995, 1999) (Fig. 1). Most of the activity comes from thrust events induced by north–south compression related to the ongoing convergence across the Himalaya. The secular velocities derived from geodetic measurements across the Nepal Himalaya show that the Main Himalayan Thrust (MHT) is locked from beneath the high range to the piedmont, where it surfaces (Fig. 1), and that it roots to the north into a subhorizontal shear zone that is creeping at about 2 cm/yr (Fig. 2a) (Bilham et al., 1997; Bettinelli et al., 2006). Most of the seismicity clusters near the updip edge of the creeping zone (Fig. 2b), in a region where, according to the modeling of the geodetic data, Coulomb stress builds up at a rate higher than about 6 kPa/yr (Cattin and Avouac, 2000; Bollinger et al., 2004). This midcrustal seismicity was also observed to coincide with a

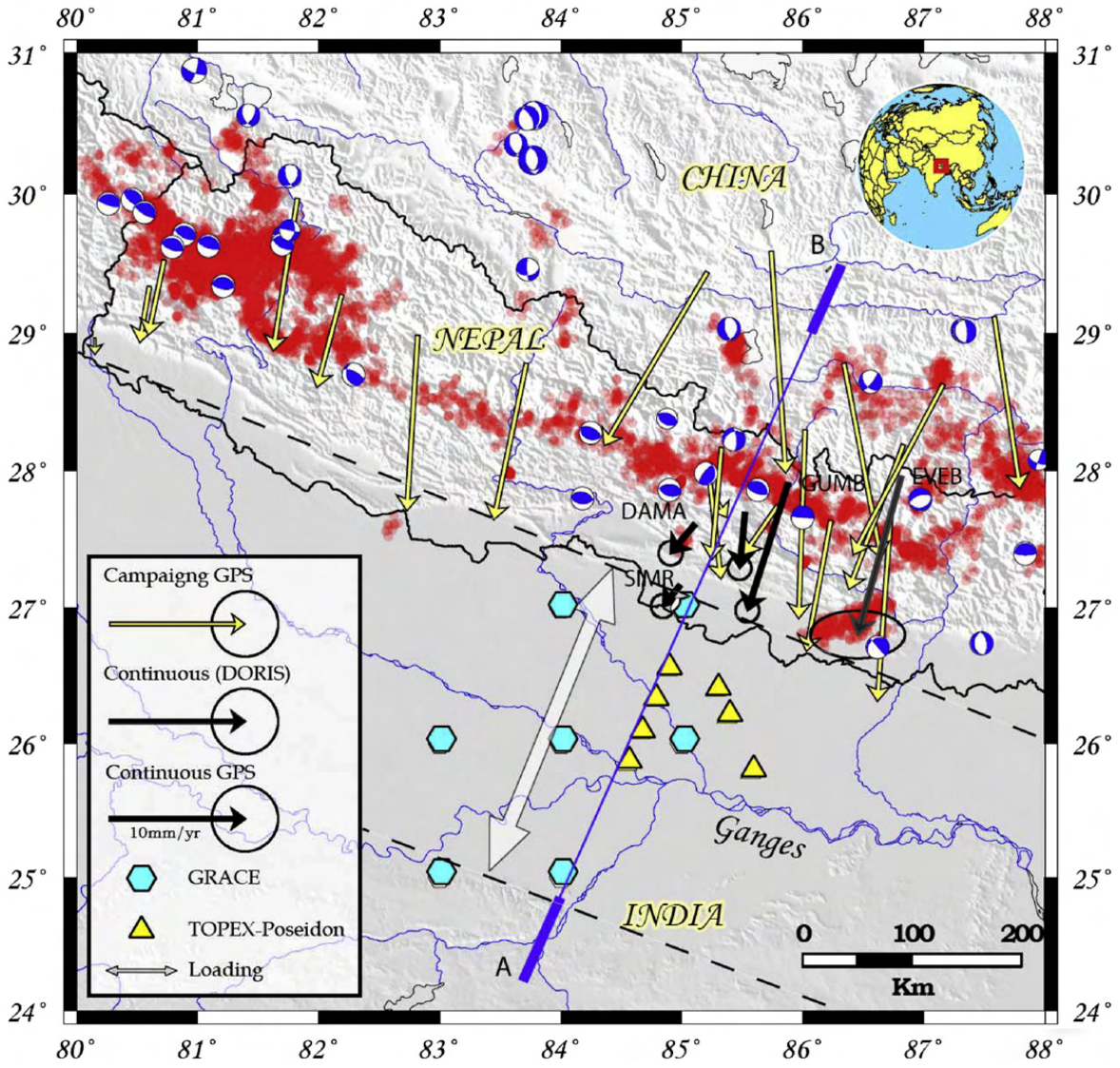

Fig. 1. Map of study area with location of data analyzed in this article. Secular velocities relative to India (Bettinelli et al., 2006) determined from campaign GPS measurements, continuous GPS measurements at SIMR, DAMA, NAGA, GUMB, and EVEB, and continuous DORIS measurements at EVEB. Also indicated are locations where free water level was determined from TOPEX-POSEIDON altimetric measurements and where aquifer levels were determined by GRACE gravimetric measurements. Seismicity was recorded by the National Seismic Center of Nepal between 04/01/1995 and 04/11/2000 (Ml>3), relocated with the double difference technique, and focal mechanism were compiled from the Harvard catalogue or determined from regional waveforms and first motions (Sudhire Rajaure, DMG/NSC; de la Torre et al., 2007). The white arrow and the dashed lines define the zone where a varying surface load, computed from the seasonal water level variations, is applied in the mechanical modeling.

zone of high electrical conductivity interpreted to reflect an interconnected fluid phase that probably comes from metamorphic dehydration of the underthrusting Indian basement (Lemmonier et al., 1999; Avouac, 2003) (Fig. 2c). This coincidence suggests some coupling between seismicity and fluids flow.

3. Seasonality of strain and seismicity

The geodetic time series (Figs. 2b, 3b and c) and seismicity (Fig. 3a) both show strong seasonal variations. Interpretation of the variations requires some care, as they could result from a variety of meteorological

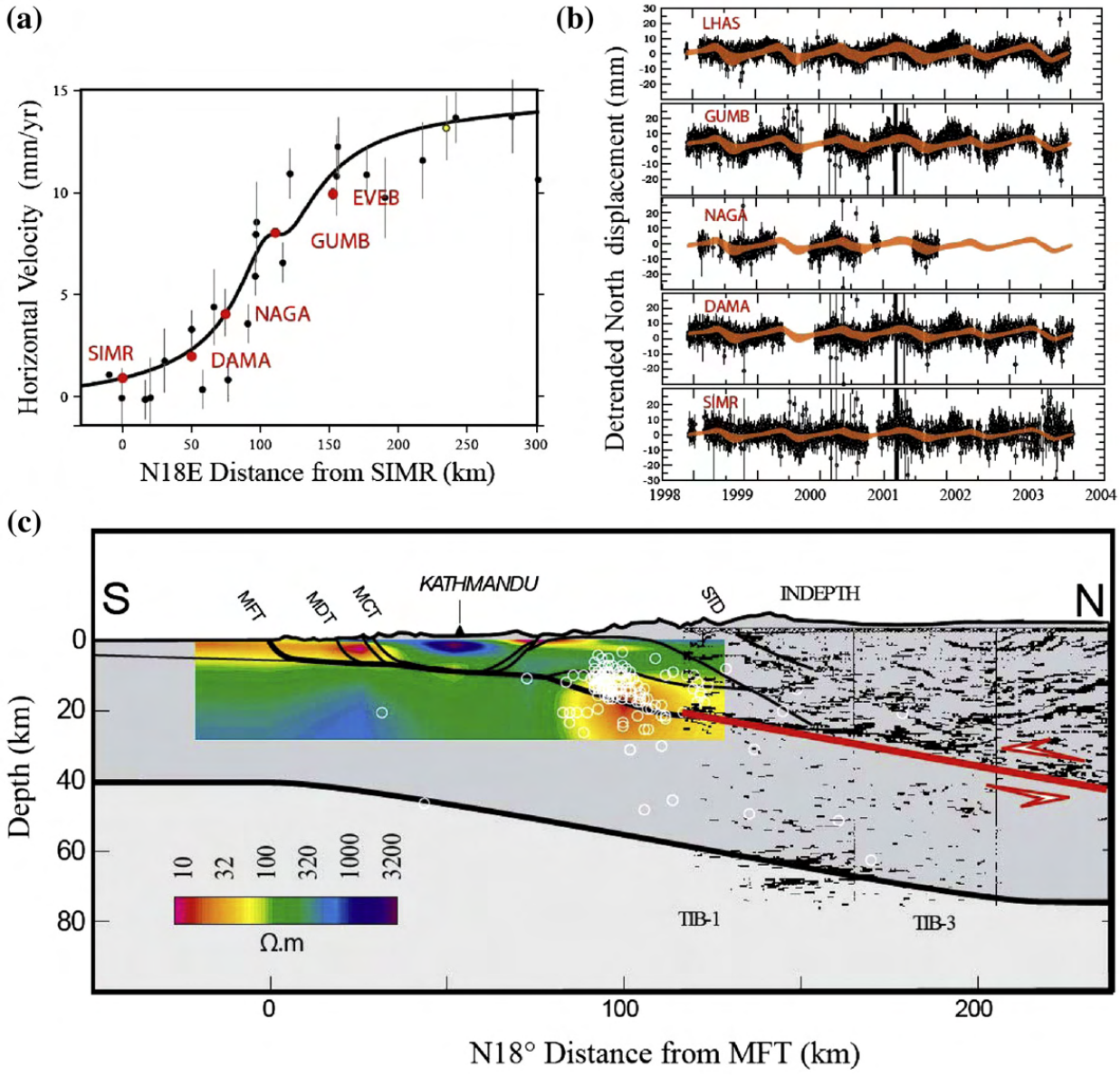

Fig. 2. Secular interseismic strain and seasonal variation across Nepal Himalaya. a Secular velocities relative to India determined from campaign measurements (black dots) and from the analysis of the time series recorded at the continuous geodetic stations (Bettinelli et al., 2006) (red dots, uncertainties are smaller than the dots size). Continuous line shows the predicted horizontal velocity for a slip rate of 16 mm/yr, a shallow dipping dislocation as indicated in cross section and derived from least-squares adjustments of all GPS and leveling data from central Nepal (Bettinelli et al., 2006). b GPS time series de-trended by removing the secular motion. The seasonal variations increase in amplitude from south to north. Details on the processing of the GPS data are given in Bettinelli et al., (2006). Red shaded areas show seasonal geodetic displacements computed from the variation of surface load due to seasonal variation of water storage (2 sigma uncertainty) assuming an elastic half space with a elastic shear modulus of 40 GPa and a Poisson coefficient of 0.25. c simplified geological cross section and geophysical constraints on the crustal structure across central Nepal. See Fig. 1 for location of section. The conductivity section was obtained from a magnetotelluric experiment carried out along section AB across central Nepal (Lemmonnier et al, 1999). Also reported are the INDEPTH seismic sections about 500 km east of section AB (Brown et al, 1996; Nelson et al, 1996; Zhao et al., 1993). All thrust faults are inferred to root at depth into a subhorizontal ductile shear zone that coincides with a prominent midcrustal reflector. White circles show seismicity corresponding to events with well-constrained hypocentral depths (Cattin and Avouac, 2000).

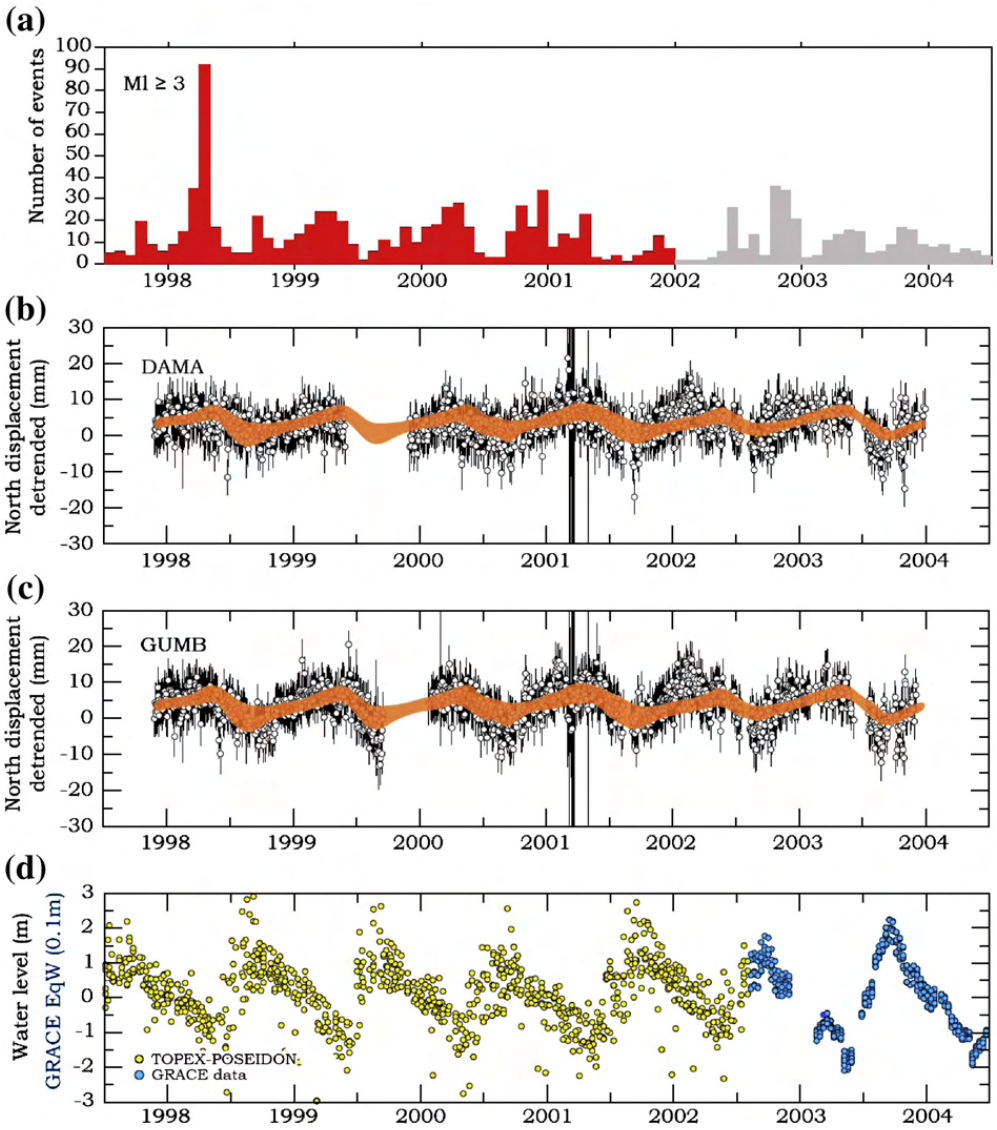

Fig. 3. Correlation between seasonal variation of seismicity, geodetic displacements and water level in the Ganges basin. a Seismicity (Ml>3) is shown in red for the period over which the geometry of the seismic network has not changed. It is shown in grey for the period over which the detection level varied due to discontinuous operation of the seismic stations (the apparent drop in January 2002 in particular is an artifact of technical failure of about 50% of the seismic stations during that winter). Variations from the secular trend of the geodetic position shown for stations DAMA (b) and GUMB (c). d Water level variations of some major rivers in the Ganges basin measured by TOPEX-Poseidon (yellow dots) and equivalent water thickness derived from GRACE (blue dots). See location of these measurements in Fig. 1. Red shaded areas in b and c show seasonal geodetic displacements computed from the variation of surface load due to seasonal variation of water storage (2 sigma uncertainty) assuming an elastic half space with a elastic shear modulus of 40 GPa and a Poisson coefficient of 0.25.

artifacts: the GPS time series might be biased by mis-correction of the tropospheric delays and seasonal variations in the seismic noise level could affect the detection threshold of the seismic network.

Analysis of a catalogue of ~10,000 earthquakes (Bollinger et al., 2007) shows that the seismicity rate in the winter is twice as high as in the summer at all magnitudes above the detection threshold (estimated to be Ml=2.0 (Pandey et al., 1999)), which rules out the possibility that the pattern arises solely from seasonal variations in seismic noise. This analysis also shows an extremely low probability—only 10^{-15} when computed with the Schuster test as applied to the declustered catalogue (Schuster, 1897; Heaton, 1975)—that this seasonality is due to chance. We have analyzed potential tropospheric bias in the GPS measurements. The details of this analysis is presented elsewhere (Bettinelli, 2007) and only summarized briefly here. We have first compared the troposphere delays estimated from the GPS data with those predicted from the only in situ meteorological data, and verify that, although these latter are not representative of the whole atmospheric

column, there is no significant discrepancy in the overall shape and amplitude (Bettinelli, 2007) (Fig. S2). The vertical positions, which are known to be particularly sensitive to tropospheric effects, do however show some correlation with the seasonal variations of tropospheric delays suggesting possible atmospheric bias. By contrast, the seasonal variations of horizontal positions are in phase neither with the tropospheric delays, the phase shift being of about 4 months, nor with the variations of vertical positions (Bettinelli, 2007). Temporal variations in the horizontal gradient of the tropospheric delay cannot be either the cause of the observed seasonal variations of horizontal positions since they also vary in phase with the tropospheric delays (Bettinelli, 2007). The horizontal strain variations derived from our GPS measurements must thus represent real ground deformation. Variations of the vertical component are less reliable. They probably reflect a combination of real ground displacement and troposheric artifacts.

The amplitude of the horizontal seasonal geodetic displacements increases northwards, so that the shortening rate across the range is lower in the summer than in the winter. This points to a local source capable of producing horizontal contraction in the winter and horizontal extension in the summer, superimposed on the secular shortening rate across the Himalaya.

4. Potential causes of seasonal strain in the Himalaya

Seasonal variations not related to tropospheric miscorrections are commonly observed in geodetic time series and may have a variety of causes (Blewitt and Lavallee, 2002; Bawden et al., 2001; Dong et al., 2002; Ben-Zion and Leary, 1986) but only few can produce the kind of seasonal strain variation reported in this study, and explain the correlated variations of geodetic strain and seismicity. One possibility is that the creep rate on the MHT, which drives interseismic shortening, varies with time due to a resonance with atmospheric seasonal forcing (Perfettini and Schmittbuhl, 2001). Such a mechanism has been invoked to explain the periodicity of slow events (Lowry, 2006; Shen et al., 2005). Another possibility is that the creep rate on the MHT is constant, but a seasonal source of loading produces stress variations capable of modulating the seismicity and geodetic strain. Thermoelastic strain has been shown to be a dominant source of seasonal strain in California (Ben-Zion and Leary, 1986; Prawirodirdjo et al., 2006) and could be invoked in the Nepal Himalaya as well. Atmospheric pressure, hydrology and snow cover can also all produce seasonal variations in surface oading, which could in turn cause seasonal variations in geodetic strain and seismicity. In Japan, for example, snow load variations produce observable seasonal geodetic displacements, and seasonal seismicity (Heki, 2003). In California, atmospheric pressure has been proposed to explain seasonal variations in seismicity following the Landers earthquake (Gao et al., 2000). In the Himalaya, snow load and atmospheric pressure are both at a maximum in the winter (Putkonen, 2004). These effects should, contrary to what is observed, inhibit thrust earthquakes in the winter (Bollinger et al., 2007).

Variation of surface loading associated with the hydrological cycle is another possible mechanism that has been shown to be capable of producing measurable geodetic strain at a regional scale (Blewitt et al., 2001; van Dam et al., 2001). We have explored more particularly this potential effect using satellite altimetry measurements from TOPEX-Poseidon and geoid data from the GRACE mission (Fig. 3d) to estimate the temporal variations of land water storage (Frappart et al., 2006). We selected TOPEX-Poseidon altimetric measurements over major rivers within the Ganges basin (Fig. 1). These measurements provide an estimate of the free surface water level to within a few tens of cm. They show that during the monsoon season the free water level over the whole Gangetic basin rises by about 4 m, starting in mid-May, reaches a maximum in early September, followed by a steady decrease until the next monsoon. Strong, in-phase, seasonal variations in seismicity, geodetic displacements and water levels in the Ganges basin suggest a striking causal relationship (Fig. 3).

The GRACE satellite measurements of the geopotential complemented the TOPEX-Poseidon observations, which ended in 2002. In addition the GRACE measurements provide an estimate of the mass surface loading due to free surface water, groundwater and soil moisture. The GRACE geoid data set consists of monthly estimates of time series of spherical harmonics up to degree and order 50, corresponding to a spatial resolution of 400 km at the surface of the Earth (Tapley et al., 2004; Tapley et al., 2004; Schmidt et al., 2006). In the process, atmospheric and oceanic tide effects are removed from the geoid harmonic coefficients. The coefficients of the contribution of continental water mass storage, including surface waters, soil moisture and groundwater, are extracted from the 10-day sampled GRACE solutions (Lemoine et al., 2007) using an iterative inverse method (Ramillien et al., 2006, 2005). Strong seasonal variations of surface load are revealed. Variation of water storage in the Ganges basin dominates the signal with a peak-to-peak amplitude of about 50 cm (Figs. 3d and 4).The radar altimetry and GRACE-derived land water time series do not overlap, but a similar phase is found in the seasonal cycle and the

amplitude of the equivalent water thickness derived from GRACE is about ten times smaller than the variations of rivers surface elevation (Fig. 3). The free surface within the major rivers and the groundwater level vary jointly over the seasonal cycle, probably due to the relatively high permeability of the clastic sediments of the Ganges basin (Fig. 3). The surface load variations over the whole period can thus be estimated by combining the radar altimetry and the GRACE-derived land water time.

5. Influence of water storage variations on strain and stress in the Himalaya

We propose that the seasonal geodetic displacements reflect a lithospheric response to the seasonal variation of hydrological surface loads (Fig. 5). This mechanism is qualitatively consistent with our geodetic observations since the surface load rises during the summer monsoon is expected to induce extension across the Himalaya, while compression should follow in the winter when the surface load decreases. For a more quantitative assessment, we modeled this effect using two different approaches. The first is based on the analytical solution of Boussinesq (1885) for deformation of an elastic half-space submitted to a surface point load (Fig. 6), an approach used in previous similar study (Grapenthin et al., 2006). This model ignores the effects of topography and of viscous deformation. The second approach uses a finite element model in which a purely elastic plate is assumed to overly a nonviscous fluid (Figs. S1 and S2). This modeling takes topography into account. In both cases, a load mimicking the effects of water level variation is applied at the surface. The spatial distribution of surface load was estimated from the

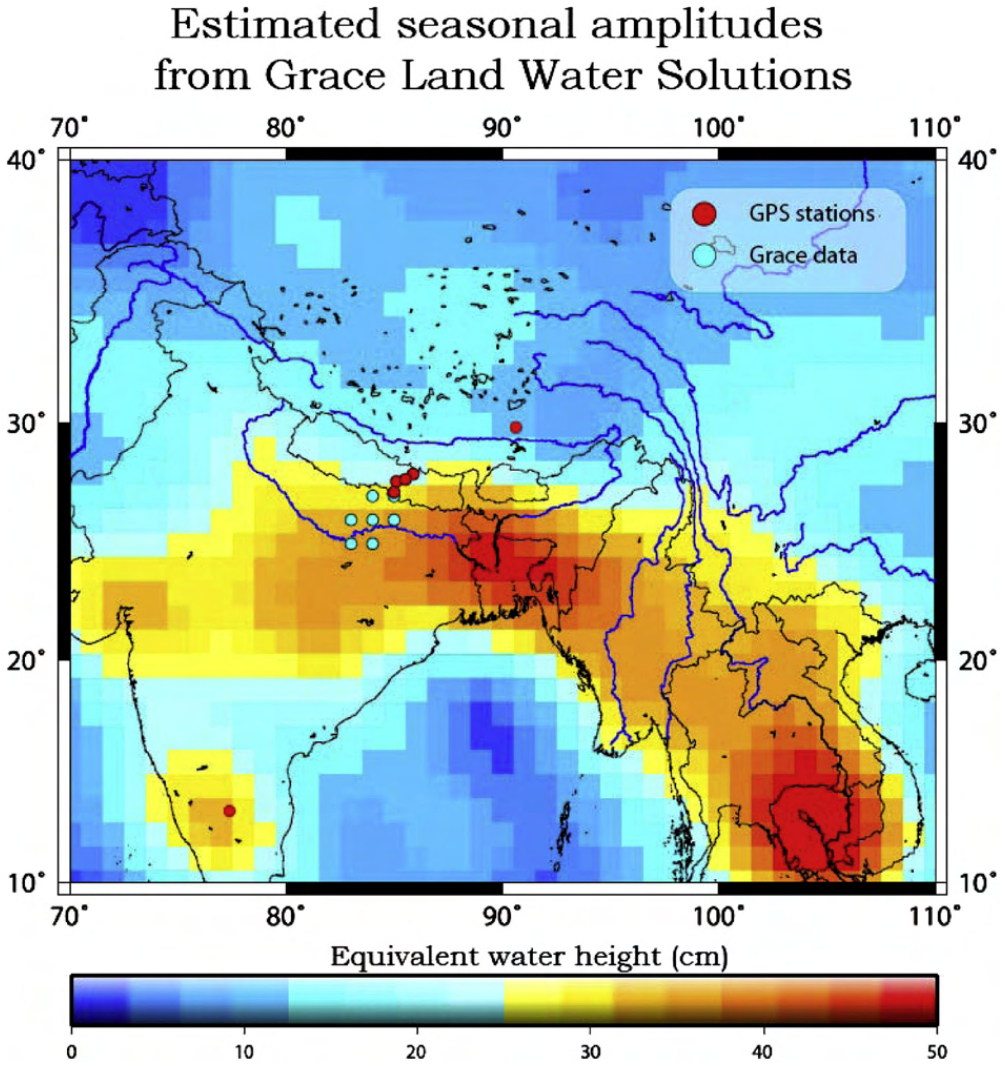

Fig. 4. Map of the seasonal peak-to-peak amplitudes of total water storage in the Southeast region, which were estimated from the GRACE Land Waters solutions up to harmonic degree 50 by linear leastsquare inversion (units: meters of equivalent-water thickness). Note the important annual variations of water mass over the Mekong and the Ganges basins that reach ±2.4 m of water height (http://www.legos.obs-mip.fr/en/equipes/gohs/resultats/c1_grace1). The dots show the locations of the GPS stations analyzed in this study.

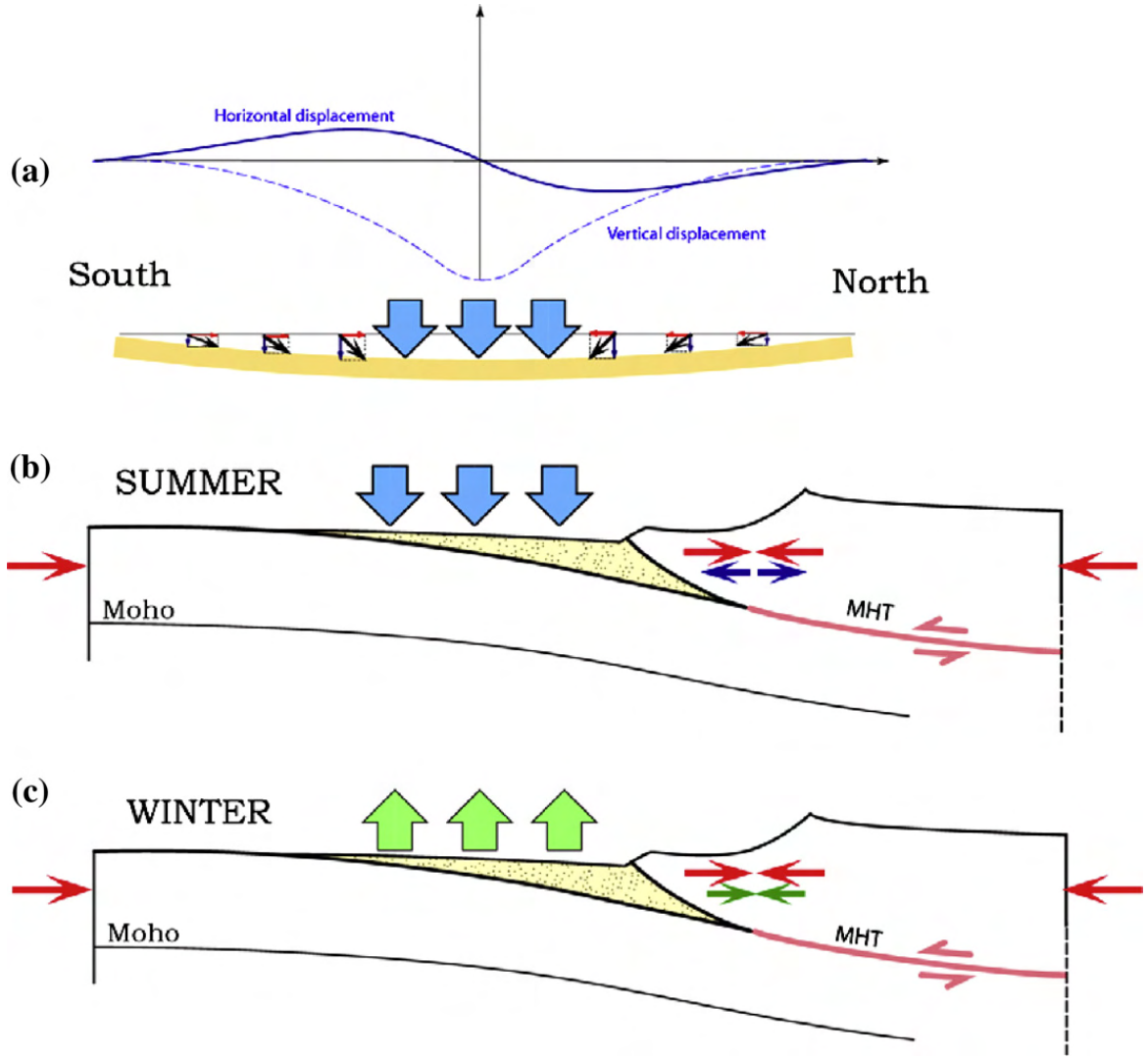

Fig. 5. Schematic diagram showing the effect of an increased water level in the Ganges basin on geodetic displacements and strain in the Himalaya. a Water level rise due to the summer monsoon increases the surface load (grey arrows), inducing elastic deformation of the crust. Subsidence and southward horizontal displacements occur north of the Ganges basin. Horizontal displacements south of the Ganges basin should be northward. b In the summer, this seasonal strain implies horizontal extension at seismogenic depth (2–15 km, blue arrows) in the Himalaya, which reduces the effect of secular horizontal compression due to interseismic strain buildup (red arrows). c The opposite occurs in the winter so that unloading, as water level drops, implies some horizontal compression (green arrows) that adds to the secular interseismic contraction (red arrows).

GRACE data and the temporal variations were estimated from combining the TOPEX-Poseidon and GRACE data (Fig. 3). The predicted seasonal displacements of both modeling approaches match the observations remarkably well (Figs. 3, 6 and S2). Although other factors might contribute to some degree, variations of water storage in the Ganges basin turns out to be the primary cause of the observed seasonality of geodetic displacements.

6. Relation between seasonal variations of stress and seismicity

This mechanism is also qualitatively consistent with the higher seismicity rate in the winter, suggesting that the gradual decrease of surface load in the Ganges induces a gradual increase of compression in the Himalaya, which adds to the effect of interseismic stress accumulation at the front of the creeping portion of the MHT (Fig. 6). To quantify the effect of stress variations on seismicity, we use the Coulomb stress, defined as $S=\tau-\mu'\cdot\sigma$, where τ is the shear stress, σ is the normal stress and μ' is an effective friction coefficient, here set to 0.3. The Coulomb stress is commonly used to evaluate whether stress variations should promote or inhibit seismicity (King et al., 1994). We find that seasonal variations in the water level of the Ganges basin induce fluctuations in the Coulomb stress computed for the zone of seismicity along the front of the high range, with a peak-to-peak amplitude of 2–4k Pa (Fig. 7). In fact, the seismicity rate is found to correlate

best with stress rate (Figs. 8 and 9), indicating that triggering of earthquakes depends on the stressing rate rather than on the absolute stress level, as has been observed in a number of previous case studies (Toda et al., 2002; Perfettini and Avouac, 2004; Hsu et al., 2006).

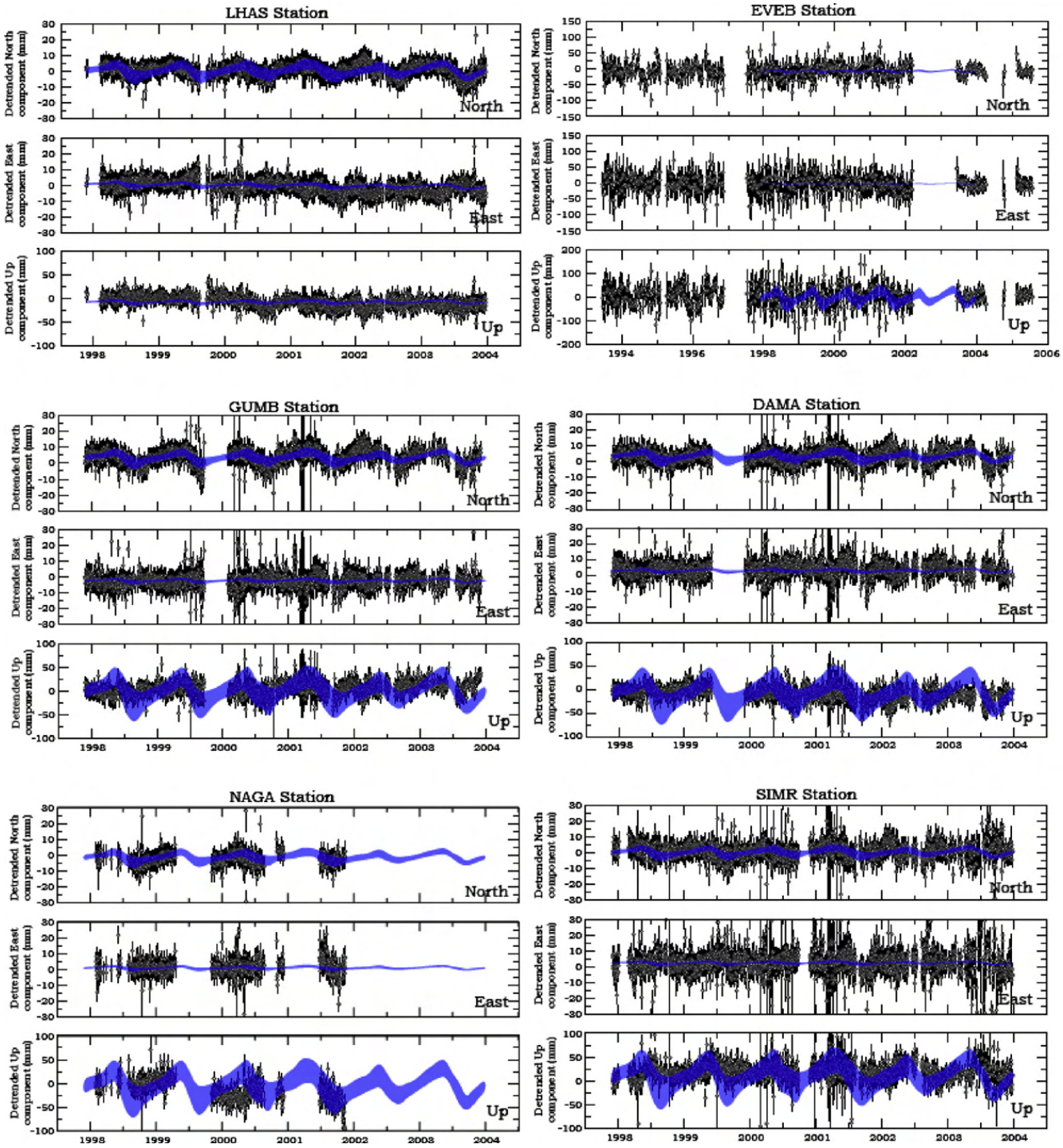

Fig. 6. Observed and predicted NS, EW and vertical displacements at stations SIMR, DAMA, GUMB, NAGA, EVEB and LHAS. Elastic half-space. The theoretical displacements were computed by convolving the distribution of surface load with the analytical solution for the deformation of an elastic half space submitted to a surface point load assuming a Young modulus of 40 GPa. [The equations originally from Boussinesq (1885) are given in standard text books on linear elasticity and can be found for example at http://www.engin.brown.edu/courses/en224/halfspace/halfspace.html]. The effect of the topography is neglected in this computation, as well as that of viscous deformation. The blue shaded areas show the seasonal geodetic displacements computed from the surface load exerted by seasonally varying water storage taking into account the spread in the GRACE and TOPEX-Poseidon measurements (shown in Fig. 3d).

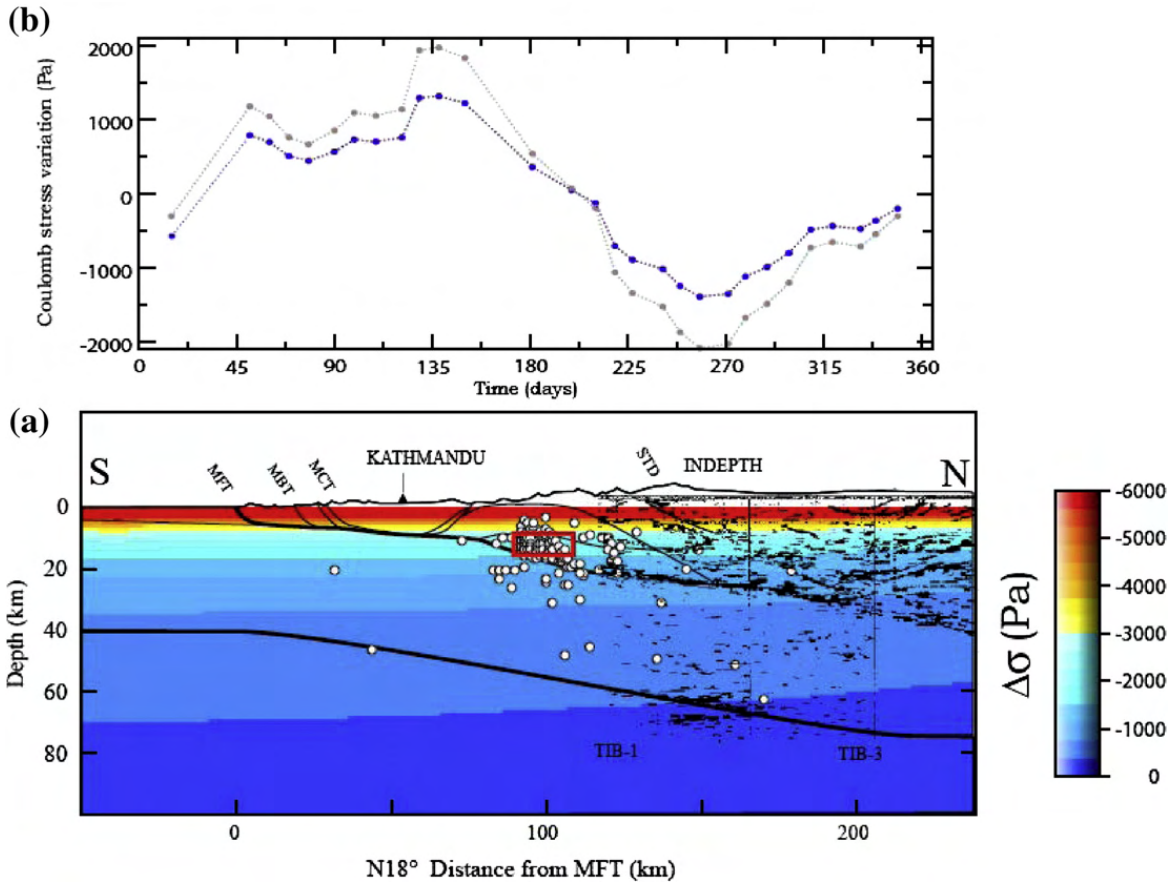

Fig. 7. Effect of seasonal variation of surface load on Coulomb stress variation. Coulomb stress is defined as $S=\tau-\mu\cdot\sigma_n$, where $\mu=0.3$ (King et al., 1994) and is computed on thrust fault dipping 30° to the north, consistent with most focal mechanisms in the seismicity cluster along the Himalayan front (Fig. 1). a Difference of Coulomb stress due to the seasonal ~4 m drop of the water level within the Ganges basin. White circles shows seismicity (Cattin and Avouac, 2000). b Temporal evolution of Coulomb stress computed at depths of 10 km (grey line) and 15 km (blue line) within the seismicity cluster. The Coulomb stress is maximum in the winter when the stored water is at minimum. It is minimum at the end of the summer monsoon, when the stored water is at maximum. The peak to peak amplitude of Coulomb stress variation within the seismicity cluster is estimated to between 2 kPa and 4 kPa.

Assuming that this linear correlation has some physical significance the sensitivity of seismicity rate to seasonal stress fluctuations can be used to estimate the secular interseismic stress rate independently of the modeling of interseismic strain. To do so, we have solved for the secular stress rate which yields the best linear correlation between the stress rate and the seismicity rate and obtained a value between 10 and 20 kPa/yr (Fig. 9). This rate represents the average stress rate within the seismicity zone along the front of the high Himalaya where stress builds up in the interseismic period around the downdip end of the locked portion of the Main Himalayan Thrust fault (Cattin and Avouac, 2000; Bollinger et al., 2004). It is likely, however, that the stress rate within this zone is highly variable depending on the geometry and complexity of the transition between the locked and creeping fault zones. The agreement between the estimate of the stress rate derived from the seasonality of seismicity and that estimated from the modeling of secular interseismic strain (>6 kPa/yr (Cattin and Avouac, 2000; Bollinger et al., 2004)) is remarkable in light of the uncertainties and approximations made in these two independent approaches.

7. Implications for earthquake nucleation

The sensitivity of Himalayan seismicity to seasonal stress and strain variations has important implications for earthquake nucleation.

We first consider a simple Coulomb failure model in which rupture occurs instantaneously when S first reaches some critical value S_c and then drops to some dynamic value S_d. In this case, if the initial Coulomb stress on various faults is random distributed between S_d and S_c, and if the fault population is subjected to a constant stress

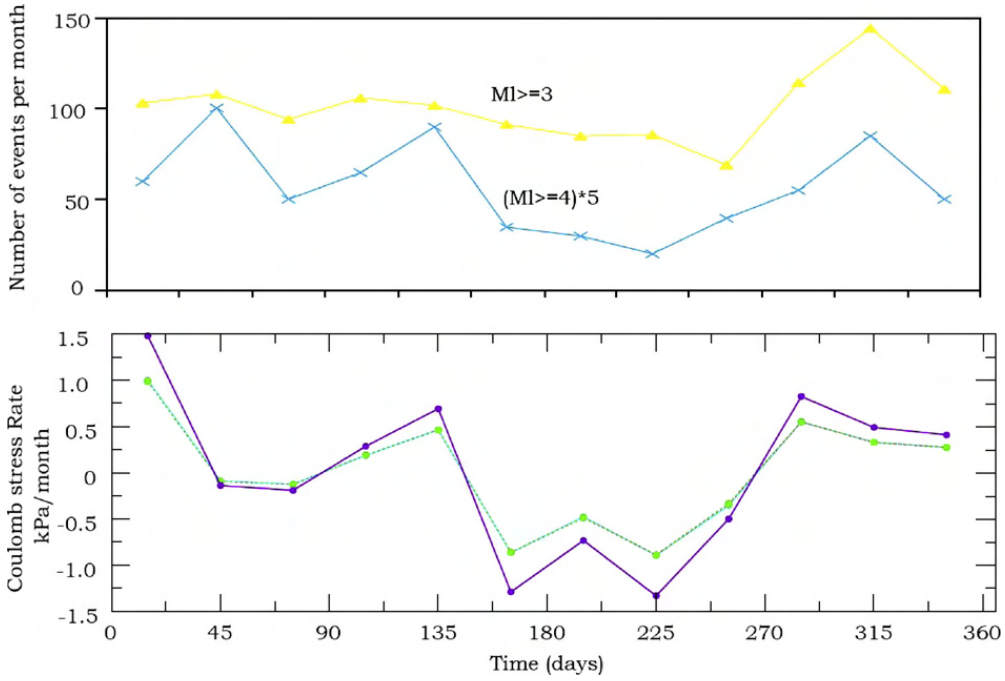

Fig. 8. Seasonal variations in seismicity rate and Coulomb stress rate. Top graph shows the average seasonal variation of seismicity between 04/01/1995 and 31/12/2001 (for Ml>3 and Ml>4) based on the declustered catalogue of (Bollinger et al., 2007). The number of events with magnitude greater than 4 has been multiplied by 5. The bottom graph shows variations in Coulomb stress rate computed at 10 km (green) and 15 km (blue) depths within the seismically active area at the front of the high range.

rate $\dot{S}_0$, then the seismicity rate r_0 is proportional to $\dot{S}_0$. Let's now consider that the system is perturbed by Coulomb stress oscillations with period T and amplitude S_m small enough that the stress rate is always positive (i.e. $\dot{S}_0 \geq 2\pi \frac{S_m}{T}$), as is the case in this study. The seismicity rate is then expected to vary in proportion to the stress rate $\dot{S}$, with periodic variations of amplitude R_m given by:

$$R_m = 2\pi \frac{S_m}{T \cdot \dot{S}_0} \cdot r_0 \quad (1)$$

This model makes it explicit that the secular stress rate, $\dot{S}_0$, can be estimated from observations of periodic variations in seismicity, and, as argued in the previous section, accounts reasonably well for the response of Himalayan seismicity to annual stress variations. Eq. (1) also suggests that the sensitivity of seismicity to periodic stress variations should increase as the period decreases, such that seismicity should be extremely sensitive to Earth tides. Indeed, Earth tides induce variations in stress on the order of 3–4 kPa, an amplitude similar to those related to the seasonal variation of surface water storage, but at a much shorter dominant period of 12 h. As already reported (Cochran et al., 2004), no clear correlation between seismicity and Earth tides is actually observed in the Himalaya however. This suggests that the response of seismicity to periodic stress perturbations is frequency dependent. This is most probably due to the fact that, at the time scale of Earth tides, the duration of earthquake nucleation is not negligible and a simple Coulomb failure model therefore does not apply (Dieterich, 1987; Lockner and Beeler, 1999; Beeler and Lockner, 2003). The duration of nucleation of earthquakes in the Himalaya is thus probably short compared to the seasonal time scale but long compared to the semi-diurnal and 14 days dominant periods of Earth tides.

Some quantitative constraints on the constitutive laws of faults might be derived from this analysis. Within the theoretical framework of rate-and-state friction (Dieterich, 1994, 1987; Beeler and Lockner, 2003; Perfettini et al., 2003), seismic rupture is preceded by a nucleation phase of self-accelerating slip with a duration characterized by

$$t_a = \frac{a\sigma}{\dot{S}}, \quad (2)$$

where σ is the normal stress and a is a constitutive parameter reflecting the dependence of the friction coefficient, $\mu = \frac{\tau}{\sigma}$, on slip velocity, V, according to

$$a = \frac{\partial \mu}{\partial \ln V}. \quad (3)$$

If the period of an oscillating stress perturbation, T, is such that $T \gg t_a$, a fault system responds as if it were obeying a simple Coulomb failure model.

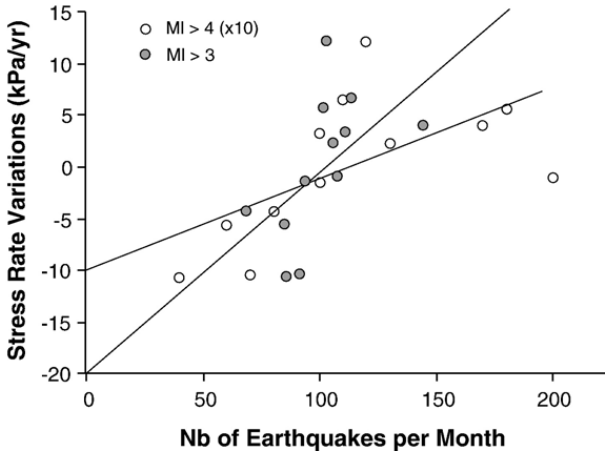

Fig. 9. Coulomb stress rate variations induced by seasonal variations of land water loading as function of seismicity rate. Purple and blue symbols correspond to earthquakes with local magnitude respectively larger than 3 and 4 (the number of Ml>4 earthquake per month was multiplied by 10). The approximately linear relationship implies a secular Coulomb stressing rate between 10 and 20 kPa/yr on average within the seismicity cluster (the secular rate reads as the intercept at the origin).

Our observations of seasonal correlation between seismicity and stress rate thus imply that t_a has to be significantly shorter than a year. Equation (3) then places an upper bound on $a\sigma$ of about 8 kPa. Due to the nucleation process, the seismicity rate should actually not respond instantaneously to a stress rate change, but instead follow a characteristic lag time on the order of t_a (Toda et al., 2002). The small lag time between seismicity rate and stress rate seasonal changes (Fig. 7) suggests that t_a is actually significantly less than 1 yr, implying a value of $a\sigma$ is less than 8 kPa.

When $T<t_a$, the sensitivity of the seismicity to stress rate variations is approximated by (Dieterich, 1987; Lockner and Beeler, 1999).

$$\frac{R_m}{r_0} = \frac{S_m}{a\sigma} \tag{4}$$

Eqs. (1) and (4) cannot be simultaneously valid except in the particular regime in which $T \approx 2\pi \cdot t_a$. In any case, Eq. (4) always provides a lower estimate of the seismicity variations expected to result from stress variations with amplitude S_m. Given that the observed seasonal variations correspond to a ratio $\frac{R_m}{r_0}$ on the order of 1/3 and that S_m is on the order of 1–2 kPa, we infer that $a\sigma$ is probably larger than 3–6 kPa.

These lines of reasoning both point to a value of $a\sigma$ on the order of 3–8 kPa. This value is about one order of magnitude less than the 0.5–10 MPa range of values estimated from postseismic creep (Perfettini and Avouac, 2004; Hsu et al., 2006; Miyazaki et al., 2004; Hearn et al., 2002). Assuming a lithostatic normal stress, the 5–15 km depth range of the seismicity implies that a is on the order of 10^{-5}, several orders of magnitude lower than the 10^{-2}–10^{-3} range of laboratory estimates (Marone, 1998). The low value of $a\sigma$ might be due to high pore pressure rather than a particularly low value of a. This possibility is supported by the high conductivity, suggesting the presence of fluids, observed in the area of seismicity (Fig. 2c). High pore pressure has also been proposed to explain the seasonal variation of seismicity following the Landers earthquake, which was observed mainly at sites with hydrothermal activity (Gao et al., 2000), and the small value of $a\sigma$, about 35 kPa, which was estimated from the temporal evolution of seismicity induced by a magmatic intrusion (Toda et al., 2002).

8. Conclusion

Permanent geodetic monitoring in the Himalaya has revealed that secular interseismic strain is modulated by strong seasonal variations dominantly driven by surface load variations of hydrological origin. Himalayan background seismicity is extremely sensitive to the small seasonal stress perturbations with a peak-to-peak amplitude of a few kPa induced by this mechanism. Given a weak sensitivity to Earth tides and an insignificant lag time between stress rate and stress rate variations, we infer that earthquake nucleation in the region takes place on a time scale longer than days but probably shorter than a few months. A nucleation phase is predicted by rate-and-state friction models of earthquake nucleation, but the short nucleation inferred here requires either that $a = \frac{\partial \mu}{\partial \ln V}$ on natural faults be on the order of 10^{-5}—orders of magnitude smaller than the values estimated from laboratory experiments—or, more probably in view of the correlation of seismicity with crustal conductivity, that earthquakes along the Himalayan front nucleate in areas of high pore pressure.

Acknowledgements

We are grateful to M.R. Pandey and all our collaborators, at NSC and DMG, and DASE at CEA, for their dedicated effort, which permitted the deployment, maintenance, and operation of the Nepal seismic network and the CGPS stations. This study has benefited from discussions with Hugo Perfettini, Jean-Paul Ampuero, Rodolphe Cattin, and Frederic Perrier, and from insightful reviews by Roland Burgman and Roger Bilham. Elisabeth Nadin is thanked for her help in editing this manuscript.

Appendix A. Supplementary data

Supplementary data associated with this article can be found, in the online version, at doi:10.1016/j.epsl.2007.11.021.

References

Avouac, J.P., 2003. In: Dmowska, R. (Ed.), Mountain building, erosion and the seismic cycle in the Nepal Himalaya. Adv. Geophys., 46. Elsevier, Amsterdam, pp. 1–79.

Bawden, G.W., Thatcher, W., Stein, R.S., Hudnut, K.W., Peltzer, G., 2001. Tectonic contraction across Los Angeles after removal of groundwater pumping effects. Nature 412, 812–815.

Beeler, N.M., Lockner, D.A., 2003. Why earthquakes correlate weakly with the solid Earth tides: effects of periodic stress on the rate and probability of earthquake occurrence. J. Geophys. Res.-Solid Earth 108.

Ben-Zion, Y., Leary, P., 1986. Thermoelastic strain in a half-space covered by unconsolidated material. Bull. Seismol. Soc. Am. 76, 1447–1460.

Bettinelli, P., Déformation intersismique de l'Himalaya du Népal à partir de données GPS, PhD, Université Paris VII(2007) 198pp.

Bettinelli, P., Avouac, J.P., Flouzat, M., Jouanne, F., Bollinger, L., Willis, P., Chitrakar, G.R., 2006. Plate motion of India and interseismic strain in the Nepal Himalaya from GPS and DORIS measurements. J Geod. 80, 567–589.

Bilham, R., Larson, K., Freymueller, J., Jouanne, F., LeFort, P., Leturmy, P., Mugnier, J.L., Gamond, J.F., Glot, J.P., Martinod, J., Chaudury, N.L., Chitrakar, G.R., Gautam, U.P., Koirala, B.P., Pandey, M.R., Ranabhat, R., Sapkota, S.N., Shrestha, P.L., Thakuri, M.C., Timilsina, U.R., Tiwari, D.R., Vidal, G., Vigny, C., Galy, A., deVoogd, B., 1997. GPS measurements of present-day convergence across the Nepal Himalaya. Nature 386, 61–64.

Blewitt, G., Lavallee, D., 2002. Effect of annual signals on geodetic velocity. J. Geophys. Res. Solid Earth 107.

Blewitt, G., Lavalee, D., Clarke, P., Nurutdinov, K., 2001. A new global mode of Earth deformation: seasonal cycle detected. Science 294, 2342–2345.

Bollinger, L., Avouac, J.P., Cattin, R., Pandey, M.R., 2004. Stress buildup in the Himalaya. J. Geophys. Res. 109. doi:10.129/2003JB002911.

Bollinger, L., Perrier, F., Avouac, J.P., Sapkota, S., Gautam, U., Tiwari, D.R., 2007. Seasonal modulation of seismicity in the Himalaya of Nepal. Geophys. Res. Lett. 34. doi:10.1029/2006GL029192.

Boussinesq, J., 1885. Application des potentiels à l'étude de l'équilibre et du mouvement des solides Ålastiques. Blanchard 1969, Reprint Paris. 1885.

Brown, L.D., Zhao, W.J., Nelson, D.K., Hauck, M., Alsdorf, D., Ross, A., Cogan, M., Clark, M., Liu, X.W., Che, J.K., 1996. Bright spots, structure, and magmatism in southern Tibet from INDEPTH seismic reflection profiling. Science 274, 1688–1690.

Cattin, R., Avouac, J.P., 2000. Modeling mountain building and the seismic cycle in the Himalaya of Nepal. J. Geophys. Res.-Solid Earth 105, 13389–13407.

Cochran, E.S., Vidale, J.E., Tanaka, S., 2004. Earth tides can trigger shallow thrust fault earthquakes. Science 306, 1164–1166.

de la Torre, T.L., Monsalve, G., Sheehan, A.F., Sapkota, S., Wu, F., 2007. Earthquake processes of the Himalayan collision zone in eastern Nepal and the southern Tibetan Plateau. Geophys. J. Int. 171, 718–738.

Dieterich, J.H., 1987. Nucleation and triggering of earthquake slip: effect of periodic stresses. Tectonophysics 144, 127–139.

Dieterich, J.H., 1994. A constitutive law for the rate of earthquake production and its application to earthquake clustering. J. Geophys. Res. 99, 2601–2618.

Dieterich, J., Cayol, V., Okubo, P., 2000. The use of earthquake rate changes as a stress meter at Kilauea Volcano. Nature 408, 457–460.

Dong, D., Fang, P., Bock, Y., Cheng, M.K., Miyazaki, S., 2002. Anatomy of apparent seasonal variations from GPS-derived site position time series. J. Geophys. Res. Solid Earth 107.

Frappart, F., Do Minh, K., L'Hermitte, J., Cazenave, A., Ramillien, G., Le Toan, T., Mognard-Campbell, N., 2006. Water volume change in the lower Mekong from satellite altimetry and imagery data. Geophys. J. Int. 167, 570–584.

Gao, S.S., Silver, P.G., Linde, A.T., Sacks, I.S., 2000. Annual modulation of triggered seismicity following the 1992 Landers earthquake in California. Nature 406, 500–504.

Grapenthin, R., Sigmundsson, F., Geirsson, H., Arnadottir, T., Pinel, V., 2006. Icelandic rhythmics: annual modulation of land elevation and plate spreading by snow load. Geophys. Res. Letters 33.

Heaton, T.H., 1975. Tidal Triggering of Earthquakes. Geophys. J. R. Astron. Soc. 43, 307–326.

Hearn, E.H., Burgmann, R., Reilinger, R.E., 2002. Dynamic of Izmit earthquake postseismic deformation and loading of the Duzce earthquake hypocenter. Bull. Seism. Soc. Am. 92, 172–193.

Heki, K., 2003. Snow load and seasonal variation of earthquake occurrence in Japan. Earth Planet. Sci. Lett. 207, 159–164.

Hsu, Y.J., Simons, M., Avouac, J.P., Galetzka, J., Sieh, K., Chlieh, M., Natawidjaja, D., Prawirodirdjo, L., Bock, Y., 2006. Frictional afterslip following the 2005 Nias-Simeulue earthquake, Sumatra. Science 312, 1921–1926.

King, G.C.P., Stein, R.S., Lin, J., 1994. Static stress changes and the triggering of earthquakes. Bull. Seismol. Soc. Am. 84, 935–953.

Lemmonier, C., Marquis, G., Perrier, F., Avouac, J.P., Chitrakar, G., Kafle, B., Sapkota, S., Gautam, U., Tiwari, D., 1999. Electrical structure of the Himalaya of central Nepal: high conductivity around the mid-crustal ramp along the MHT. Geophys. Res. Lett. 26, 3261–3264.

Lemoine, J.-M., Bruisma, S., Loyer, S., Biancale, R., Marty, J.-C., Perosanz, F., Balmino, G., 2007. Static and temporal gravity field models inferred from GRACE data. J. Adv. Space Res. 39, 1620–1629.

Lemonnier, C., Marquis, G., Perrier, F., Avouac, J.P., Chitrakar, G., Kafle, B., Sapkota, S., Gautam, U., Tiwari, D., Bano, M., 1999. Electrical structure of the Himalaya of central Nepal: high conductivity around the mid-crustal ramp along the MHT. Geophys. Res. Lett. 26, 3261–3264.

Lockner, D.A., Beeler, N.M., 1999. Premonitory slip and tidal triggering of earthquakes. J. Geophys. Res.-Solid Earth 104, 20133–20151.

Lowry, A.R., 2006. Resonant slow fault slip in subduction zones forced by climatic load stress. Nature 442, 802–805.

Marone, C., 1998. Laboratory-derived friction laws and their application to seismic faulting. Annu. Rev. Earth Planet. Sciences 26, 643–696.

Miyazaki, S., Segall, P., Fukuda, J., Kato, T., 2004. Space time distribution of afterslip following the 2003 Tokachi-oki earthquake: implications for variations in fault zone frictional properties. Geophys. Res. Lett. 31.

Nelson, K.D., Zhao, W.J., Brown, L.D., Kuo, J., Che, J.K., Liu, X.W., Klemperer, S.L., Makovsky, Y., Meissner, R., Mechie, J., Kind, R., Wenzel, F., Ni, J., Nabelek, J., Chen, L.S., Tan, H.D., Wei, W.B., Jones, A.G., Booker, J., Unsworth, M., Kidd, W.S.F., Hauck, M.,

Alsdorf, D., Ross, A., Cogan, M., Wu, C.D., Sandvol, E., Edwards, M., 1996. Partially molten middle crust beneath southern Tibet: synthesis of project INDEPTH results. Science 274, 1684–1688.

Pandey, M.R., Tandukar, R.P., Avouac, J.P., Lave, J., Massot, J.P., 1995. Interseismic strain accumulation on the Himalayan crustal ramp (Nepal). Geophys. Res. Lett. 22, 751–754.

Pandey, M.R., Tandukar, R.P., Avouac, J.P., Vergne, J., HÅritier, T., 1999. Seismotectonics of Nepal Himalayas from a local seismic network. J. Asian Earth Sci. 17, 703–712.

Perfettini, H., Schmittbuhl, J., 2001. Periodic loading on a creeping fault: implications for tides. Geophys. Res. Lett. 28, 435–438.

Perfettini, H., Avouac, J.P., 2004. Postseismic relaxation driven by brittle creep: a possible mechanism to reconcile geodetic measurements and the decay rate of aftershocks, application to the Chi-Chi earthquake. Taiwan, J. Geophys. Res.-Solid Earth 109.

Perfettini, H., Schmittbuhl, J., Cochard, A., 2003. Shear and normal load perturbations on a two-dimensional continuous fault: 2. Dynamic triggering. J. Geophy. Res. Solid Earth 108 art. no.-2409.

Prawirodirdjo, L., Ben-Zion, Y., Bock, Y., 2006. Observation and modeling of thermoelastic strain in Southern California Integrated GPS Network daily position time series. J. Geophys. Research Solid Earth 111.

Putkonen, J.K., 2004. Continuous snow and rain data at 500 to 4400m altitude near Annapurna, Nepal, 1999–2001. Arct. Antarct, Alp. Res. 36, 244–248.

Ramillien, G., Frappart, F., Cazenave, A., Guntner, A., 2005. Time variations of land water storage from an inversion of 2years of GRACE geoids. Earth Planet. Sci. Lett. 235, 283–301.

Ramillien, G., Frappart, F., Guntner, A., Ngo-Duc, T., Cazenave, A., Laval, K., 2006. Time variations of the regional evapotranspiration rate from Gravity Recovery and Climate Experiment (GRACE) satellite gravimetry. Water Resour. Res. 42.

Schmidt, R., Schwintzer, P., Flechtner, F., Reigber, C., Guntner, A., Doll, P., Ramillien, G., Cazenave, A., Petrovic, S., Jochmann, H., Wunsch, J., 2006. GRACE observations of changes in continental water storage. Glob. Water Change 50, 112–126 doi:110.1026/j.gloplacha.2004.1011.1018.

Schuster, A., 1897. On lunar and solar periodicities of earthquakes. Proc. R. Soc. London 61, 455–165.

Shen, Z.K., Wang, Q.L., Burgmann, R., Wan, Y.G., Ning, J.Y., 2005. Pole-tide modulation of slow slip events at circum-Pacific subduction zones. Bull. Seismol. Soc. Am. 95, 2009–2015.

Stein, R.S., 1999. The role of stress transfer in earthquake occurrence. Nature 402, 605–609.

Tapley, B.D., Bettadpur, S., Watkins, M., Reigber, C., 2004a. The gravity recovery and climate experiment: mission overview and early results. Geophys. Res. Lett. 31.

Tapley, B.D., Bettadpur, S., Ries, J.C., Thompson, P.F., Watkins, M.M., 2004b. GRACE measurements of mass variability in the Earth system. Science 305, 503–505.

Toda, S., Stein, R.S., Sagiya, T., 2002. Evidence from the AD 2000 Izu islands earthquake swarm that stressing rate governs seismicity. Nature 419, 58–61.

van Dam, T., Wahr, J., Milly, P.C.D., Shmakin, A.B., Blewitt, G., Lavallee, D., Larson, K.M., 2001. Crustal displacements due to continental water loading. Geophys. Res. Lett. 28, 651–654.

Zhao, W., Nelson, K.D., project INDEPTH Team, 1993. Deep seismic-reflection evidence continental underthrusting beneath southern Tibet. Nature 366, 557–559.